Published in final edited form as:

Ann Biomed Eng. 2011 June ; 39(6): 1620–1631. doi:10.1007/s10439-011-0267-8.

High Fluid Shear Stress and Spatial Shear Stress Gradients Affect Endothelial Proliferation, Survival, and Alignment

Jennifer M. Dolan[1,2,3], **Hui Meng**[1,2,4,5], **Sukhjinder Singh**[1,4], **Rocco Paluch**[6], and **John Kolega**[3,1]

1

2

3

4

5

6

Abstract

Cerebral aneurysms develop near bifurcation apices, where complex hemodynamics occur: Flow impinges on the apex, accelerates into branches, then slows again distally, creating high wall shear stress (WSS) and positive and negative spatial gradients in WSS (WSSG). Endothelial responses to these kinds of high WSS hemodynamic environments are not well characterized. We examined endothelial cells (ECs) under elevated WSS and positive and negative WSSG using a flow chamber with constant-height channels to create regions of uniform WSS and converging and diverging channels to create positive and negative WSSG, respectively. Cultured bovine aortic ECs were subjected to 3.5 and 28.4 Pa with and without WSSG for 24 and 36 h. High WSS inhibited EC alignment to flow, increased EC proliferation assessed by bromodeoxyuridine incorporation, and increased apoptosis determined by terminal deoxynu-cleotidyl transferase dUTP-mediated nick-end labeling. These responses to high WSS were either accentuated or ameliorated by WSSG: Positive WSSG (+980 Pa/m) inhibited alignment and stimulated proliferation and apoptosis, whereas negative WSSG (−1120 Pa/m) promoted alignment and suppressed proliferation and apoptosis. These results demonstrate that ECs discriminate between positive and negative WSSG under high WSS conditions. EC responses to positive WSSG may contribute to pathogenic remodeling that occurs at bifurcations preceding aneurysm formation.

Keywords

Wall shear stress; Wall shear stress gradient; Apoptosis; Aneurysm

Address correspondence to John Kolega, Department of Pathology & Anatomical Sciences, School of Medicine & Biomedical Sciences, State University of New York at Buffalo, 206A Farber Hall, 3435 Main Street, Buffalo, NY 14214, USA. kolega@buffalo.edu.

INTRODUCTION

As the inner most layer of the arterial wall, vascular endothelial cells (ECs) are directly exposed to the mechanical forces exerted by flowing blood. ECs are known sensors of wall shear stress (WSS),[7,8] the frictional drag force created by fluid flowing over the luminal surface of the vessel. Previous research on endothelial responses to flow has focused on the physiological baseline values of straight arterial segments (1.5–3.0 Pa) or relatively low WSS (0.1– 0.5 Pa).[13,47] These values are relevant to atherogenesis which tends to occur in low flow regions that experience disturbed flow or flow recirculation and reat-tachment. Such regions also experience high oscillating shear index and WSS gradients (WSSGs). Flow chambers incorporating a backward facing step have been used to generate recirculation zones in which ECs are exposed *in vitro* to combined low WSS and high WSSG. In this hemodynamic environment, ECs display increased permeability,[31] migration,[10,40] proliferation,[40] and activation of transcription factors.[29] In endothelia subjected to impinging flow in a T-shaped chamber, increased migration and disruption of orientation are observed in cells immediately adjacent to the impingement, where WSS is low and WSSG is high.[33,39] LaMack *et al*.[18] used converging-flow chamber to demonstrate that expression of the atherogenic genes, ICAM, MCP1, and c-jun, may be modulated by WSSG alone or through an interaction of WSS and WSSG. Thus, under low flow conditions, the presence of WSSG may exacerbate EC responses.

Although a plethora of information has been gathered about the effects of low WSS magnitudes on EC behavior, considerably less is known about EC responses to substantially higher WSS values (>5 Pa). Such high WSS occurs in arteries feeding arteriovenous fistulae,[19] the throats of stenoses,[34] and collateral arteries secondary to arterial block-ages[35,43]—situations that stimulate circumferential growth. Even higher WSS magnitudes, upwards of 30 Pa, exist chronically adjacent to the apices of bifurcations and along outer curvatures of vessels[1,22]—locations where cerebral aneurysms preferentially form.[17] Despite the critical role of such elevated WSS in flow-mediated vascular remodeling, the endothelial responses to these conditions are not well characterized. Furthermore, it has recently become apparent that WSSG affects vascular remodeling in high WSS environments. In surgically created bifurcations in dogs[26,45] and in the basilar terminus of rabbits exposed to increased flow,[25,28] Meng *et al*. have shown matrix degradation and cell loss specifically localized to regions of accelerating flow, where WSS is high and WSSG is positive. Furthermore, adjacent regions experiencing equally high WSS but *decelerating* flow, i.e., a negative WSSG, remain undamaged, suggesting that the endothelium responds differently to positive and negative WSSG. Interestingly, locations where aneurysms tend to form in the cerebral vasculature are regions where the vessel wall experiences high WSS and positive WSSG. However, the effects of WSSG on ECs have not been extensively studied, particularly in high WSS conditions, and the impact of positive vs. negative gradient is largely unknown.

To elucidate the effects of high WSS and positive and negative WSSG on ECs, we designed and constructed an *in vitro* flow system with a gradient chamber. The chamber consists of four distinct regions of tapered or parallel flow channels, such that ECs are exposed to well-defined WSSG regimes and varying WSS. Using this device, we examined how

fundamental EC responses—cell morphology, alignment, DNA replication, and programmed cell death—are affected by high WSS as well as positive and negative WSSG.

MATERIALS AND METHODS

Design of Gradient Chamber

Our goal was a chamber with separate regions of constant positive WSSG and constant negative WSSG over a range of high WSS values and with an area in each region for sufficient ECs for experimental analysis. A flow channel with parallel walls has uniform WSS; varying the height or width varies the WSS and creates WSSG. In a channel of constant height, shear stress, τ, is given by:

$$\tau = \frac{6\mu Q}{wh^2}, \quad (1)$$

where μ is the viscosity, Q volumetric flow rate, w channel width, and h channel height.[2] This equation is valid for Newtonian fluid under fully developed laminar flow in channels with a high aspect ratio ($w \gg h$), so the roof of the chamber channel was made wide and low. WSSG is the derivative of τ as a function of distance, x, along the channel:

$$\frac{d\tau}{dx} = -\frac{12\mu Q}{wh^3}\frac{dh}{dx}. \quad (2)$$

Integrating Eq. (2) with the initial condition $h = h_0$ at $x = 0$, gives the channel height profile, $h(x)$, required to produce a constant shear stress gradient of $d\tau/dx$:

$$h = \frac{h_0}{\sqrt{1 + \frac{wh_0^2}{6\mu Q}\frac{d\tau}{dx}x}} \quad (3)$$

From this, we estimated chamber dimensions that would give appropriate WSS, WSSG, and area for ECs. Exact WSS and WSSG distributions were then determined by computational fluid dynamic (CFD) simulations as described in Szymanski *et al*. except that extruded quad meshes were used as computational grids. Dimensions were then further modified as necessary. The final design iteration (Fig. 1a) used a steady flow rate of 2.0 L/min, constant chamber width of 22 mm, and varying height, with a parallel section (h = 3 mm), converging section, narrower parallel section (h = 1 mm), diverging section recovering the original height (h = 3 mm), and a final parallel section. This created, respectively, a WSS with no gradient, positive WSSG, higher WSS with no gradient, negative WSSG, and the first WSS with no gradient again.

The flow chamber was constructed of silicone elastomer (Sylgard) in two pieces, formed in molds produced with computer numerical control machining based on ProEngineer geometry. The top piece formed the flow channel with the specified geometry, and the bottom was flat with rectangular recesses to hold the microscope coverglasses with ECs.

The chamber halves were held together between two polycarbonate plates fastened with hex socket cap screws.

In Vitro Flow Loop

The flow chamber was connected to a flow loop[27] consisting of reservoir, peristaltic pump, and three fluid capacitors to dampen pulsatility. The flow rate was monitored using an ultrasonic flow probe (Transonic Systems), and the systemic pressure of the system was measured to be approximately 100 mmHg using a pressure transducer just upstream of the entrance to the cell chamber (Becton–Dickinson).

Cell Culture

Bovine aortic ECs were cultured as previously described[27,39] and used at passages 15 and 16 for flow experiments. These cells maintain their endothelial phenotype as indicated by expression of Factor VIII, PECAM-1, eNOS, and VEGF receptor; binding of LDL; formation of monolayers that maintain barrier function as demonstrated by electric resistance and protein permeability assays; tube formation on matrigel; and angiogenesis-like migration in collagen gels [14,15,21,24,27] BAECs were seeded on sterilized uncoated Fisherbrand® Microscope Cover Glass (Fisher Scientific) at approximately 25% confluence and allowed to grow to confluence for 5–6 days before exposure to flow. 24 h before flow exposure, the culture medium was replaced with culture medium containing dextran (Sigma) to increase the viscosity of the media to 3.5 cP at 37 °C, equivalent to that of blood. This medium was used as the perfusion fluid in all flow experiments.

Morphological Examination

After flow exposure, ECs were viewed under a phase contrast microscope (Ziess Axiovert 40) to confirm that the monolayer remained adherent to the coverglass. Cells were then fixed in 1% paraformaldehyde, and digital images were acquired using a Ziess Axio Observer inverted microscope with a Ziess camera and AxioVision LE software. EC orientation was quantified in Image-J using a Fourier analysis originally described by Chaudhuri *et al.*[6] to quantify the orientation of collagen fibers. Briefly, a 512 × 512 region of interest padded with the mean grayscale value of the image was created, and the Fourier transform of the entire image was computed. A directional filter was applied in Fourier space, passing only angular orientations between 0° and 10°, and then an inverse transform was performed. The total intensity remaining in the final filtered image was summed, and the process repeated after rotating the filter in 10° increments, through 180°. Cell alignment was quantified by an alignment index similar to that described by Ng *et al.*[30]: the intensity within ±10° of the direction of flow was divided by the fraction of the total intensity that would lie within this range for a uniform, randomly oriented population (20°/180° = 0.11), and 1 was subtracted so that random distribution (no orientation) had a value of zero. The index was then normalized by the value for cells subjected to 3.5 Pa, under which ECs align parallel to flow. Thus, a value of 1 represents alignment in the flow direction equivalent to cells under 3.5 Pa, and a value of 0 represents no preferential alignment in the direction of flow.

Apoptosis-Proliferation Staining

Apoptotic ECs were stained using a terminal deoxynucleotidyl transferase dUTP-mediated nick-end labeling (TUNEL) Apoptosis Detection Kit (Chemicon International) with diaminobenizidine (DAB) visualization. Proliferating ECs were identified by bromodeoxyuridine (BrdU) incorporation. Two hours before ending the flow experiment, BrdU labeling reagent (1:1000) was added to the flow loop and to static controls. At the end of the experiment, cells were fixed, permeabilized, and stained for BrdU using a commercial monoclonal immunofluorescence kit (Roche). Diamidino-2-phenylindole dihydrochloride (DAPI) was included in the mounting medium to stain nuclei for enumeration of total cells.

Cell Imaging

A composite image of each EC monolayer was created by stitching together images taken at 10× magnification over the entire length of the coverglass with a Ziess Axio Imager Zi. The height of the composite image was 2–4 mm, the width was equal to the length of the coverslip (50 mm), and the image was centered within ±5 mm of the centerline of the coverslip so as to exclude cells near the channel's edges. Using Image-J software, the image was divided into 200-lm long regions of interest (ROIs) within which cells that were positively stained for apoptosis or proliferation were counted and percentages determined based on DAPI-stained nuclei, which gave the total number of cells in each region. A minimum of five ROIs were averaged for every WSS increment of 2.5 Pa.

Statistical Analysis

Each experiment was performed at least three times and all values represented as means ± standard error. In order to account for interdependence of data collected within each of the experiments, difference among means was performed using Mixed Model ANOVA with the SAS Proc Mixed procedure (SAS Institute).

RESULTS

Flow Dynamics in the Chamber

The flow chamber was operated with a constant flow rate of 2 L/min, which produced Reynolds numbers ranging from 780 to 848. CFD simulations confirmed that flow was laminar and revealed a very small re-circulation zone at the roof of the chamber at the exit of the diverging region. However, the recirculation was confined to the top 0.5 mm of the maximum channel height (3 mm) and did not affect flow at the culture surface. Figure 1b shows that the streamlines at the cell culture surface were highly parallel to the long axis of the channel, with only slight deviations near the very edges of the channel. The accompanying map of the pressure on the culture surface shows a gradual drop of less than 20 mmHg across the entire cell chamber and less than 5 mmHg across any of the four test sections (Fig. 1b). CFD also provided the local WSS and WSSG values at each location in the flow channel (Fig. 2):

1. The initial parallel section has a WSS of 3.5 Pa and no gradient. Physiological baseline WSS in straight vessels varies in the arterial system within a range of 1–7 Pa over the cardiac cycle[12,23,37] with time averaged WSS being between 1.5 and

2.5 Pa. WSS of 3.5 Pa is slightly higher than the average baseline WSS, but low relative to the WSS adjacent to bifurcation apices. We used this as the low end of our examination of high WSS effects.

2. The second parallel section has high WSS of 28.4 Pa and no gradient. This value was chosen based on CFD simulations of the human basilar terminus and of human internal carotid artery and middle cerebral artery bifurcations which indicate that maximum WSS near the apices of these bifurcations ranges from 11 to 34 Pa.[1,22]

3. In the converging section, WSS increases from 3.5 to 30 Pa, producing a positive gradient. At the entrance, there is a spike in WSSG due to the transition from uniform to converging height. After this discontinuity, the change in height follows Eq. (3). Over the segment where WSS increases from 12.4 to 28.3 Pa, the WSSG is maintained at a constant positive value of 980 Pa/m. The constant gradient region is 16.2 mm in length. WSS peaks at 30 Pa but recovers to 28.4 Pa as flow exits the converging section.

4. In the diverging section, WSS decreases monotonically from 28.4 down to 1.0 Pa to produce a negative WSSG. There is an initial dip in WSSG due to the discontinuity in WSS when the channel height transitions into the divergence. Past this discontinuity, WSS decreases monotonically from 22.5 to 6.6 Pa. Over this range of WSS values, the WSSG is a constant negative gradient of 1120 Pa/m. The constant negative WSSG region is 14.2 mm in length. WSS recovers to 3.5 Pa as flow exits the diverging section.

These four regions expose ECs to two uniform WSS values in the absence of a WSS gradient and to one uniform positive WSSG and one uniform negative WSSG, both over a range of WSS in between the two no-gradient WSS values. Because the WSSG over the WSS range of 12.5–22.5 Pa in the tapered sections are constant and of similar magnitude but opposite sign, comparison between these two regions reveals effects that can be attributed solely to differences between positive and negative WSSG.

High WSS Alone Decreases EC Alignment and Density

To examine EC responses to high WSS, we compared cells in the two parallel channel sections. Immediately following 24 h of flow exposure, microscopic examination revealed striking differences in cell alignment between 3.5 and 28.4 Pa (Fig. 3). ECs exposed to 3.5 Pa oriented with their long axes parallel to the flow direction within 24 h (Fig. 3a) and maintained this alignment at longer times (Fig. 3d). Under 28.4 Pa, however, alignment was inhibited: cells were poorly aligned at 24 h (Fig. 3b) and 36 h (Fig. 3e), although cells did show more alignment at 36 h. This was confirmed quantitatively (Figs. 3c, 3f): The alignment index for cells under 28.4 Pa significantly increased between 24 and 36 h ($p = 0.04$), but remained significantly lower than that of cells under 3.5 Pa at both time points ($p < 0.0001$ and $p = 0.007$, respectively). A similar delay in alignment has previously been reported for ECs under lower WSS of 10 Pa[27] and 12.8 Pa.[44]

Cell density was also lower after 24 h under WSS of 28.4 Pa than under 3.5 Pa (Fig. 4; $p < 0.0001$). Although density was lower, the vast majority of cells remained adherent under

28.4 Pa, as cell density was within 10% of that under 3.5 Pa. Use of coverglass rather than standard slide glass was critical for cell adhesion under high WSS. This presumably reflects different surface properties of the glass, as the critical surface tension of the coverglass was 33.3 mN/m and only 22.8 mN/m for glass slide, which did not support adhesion at high WSS. Baier[3] has reported that cells attach poorly to surfaces with critical surface tension between 20 and 30 mN/m.

In addition to delaying alignment and reducing cell density, high WSS stimulated EC proliferation and apoptosis. WSS of 28.4 Pa promoted EC proliferation at 24 h as indicated by BrdU incorporation (Fig. 5a; $p = 0.002$). The percentage of proliferating cells was 2.5-fold higher than cells exposed to 3.5 Pa (12 vs. 4.75%). TUNEL staining indicated that the percentage of apoptotic cells also increased between 3.5 and 28.4 Pa (Fig. 5b; $p = 0.02$). The simultaneous stimulation of proliferation and apoptosis, coupled with reduced cell density under high WSS, suggests that the high WSS condition increases EC turnover.

Positive WSSG Inhibits and Negative WSSG Promotes Flow-Induced EC Alignment

After looking at responses to WSS alone, we investigated the effects of positive and negative WSSG by examining ECs in the converging and diverging sections of the chamber. As expected from looking at the extremes of WSS (3.5 and 28.4 Pa) without WSSG, there was a general trend that EC alignment to flow decreased with increasing WSS at both 24 and 36 h (Fig. 6). However, ECs under positive WSSG were less aligned than those under negative WSSG in almost all regions (e.g., compare Figs. 6a and 6d with 6b and 6e). At 24 h, these differences were significant where WSS was 12.5–15, 17.5–20, and 25–27.5 Pa. ($p < 0.0001$, $p = 0.04$, and $p = 0.05$, respectively). At 36 h, the difference between positive and negative gradient became more pronounced and was statistically significant for all WSS values from 5 to 20 Pa (for WSS of 5–7.5 Pa, $p = 0.05$; 7.5–10 Pa, $p = 0.02$; 10–12.5 Pa, $p = 0.01$; 12.5–15 Pa, $p = 0.02$; 15–17.5 Pa, $p = 0.01$; 17.5–20 Pa, $p = 0.03$). Note that for the regions where WSS is between 12.5 and 22.5 Pa, the positive and negative WSSGs are constant and of similar magnitude, differing only in sign. Specifically within these regions (dashed box), ECs in negative gradient (WSSG = −1120 Pa/m) were well aligned for WSS up to 20 Pa, whereas cells under positive gradient (WSSG = + 980 Pa/m) were poorly aligned. This suggests that positive WSSG inhibited EC alignment to flow while negative WSSG promoted it. However, above 20 Pa, the inhibitory effect of WSS on alignment dominates any modulation by WSSG, as cells were poorly aligned under both positive and negative WSSG.

Positive WSSG Reduces EC Number

In addition to suppressing cell alignment, positive WSSG, but not negative WSSG, reduced cell density. ECs exposed to negative WSSG for 24 h had a similar density to those exposed to a WSS of 3.5 Pa and no gradient. This was true across the entire negative WSSG region even in the highest WSS range of 25–27.5 Pa (Fig. 7). In contrast, ECs exposed to positive WSSG had a lower density similar to that occurring under high WSS (28.4 Pa) without a gradient, even at the lowest WSS in the gradient region, where WSS was only 5–7.5 Pa. Specifically comparing segments of the two gradient regions where the monolayer was subjected to the exact same WSS values, there were 13–30% fewer cells in the portion

subjected to positive WSSG than in the equivalent portion under negative WSSG. This difference was significant for all values of WSS, including the two regions over which the gradient was constant at +980 Pa/m or 21120 Pa/m (for WSS of 12.5–15 Pa, $p < 0.0001$; 15–17.5 Pa, < 0.0001; 17.5–20 Pa, $p < 0.0001$; 20–22.5 Pa, $p = 0.0003$).

To better understand the differences in cell density under positive and negative WSSG, we examined the effects of WSSG on EC proliferation and apoptosis (Fig. 8). The percentage of proliferating cells increased with increasing WSS under positive WSSG, as expected given that proliferation is higher at 28.4 Pa than at 3.5 Pa in the absence of gradient (Fig. 8a). However, cells under negative WSSG responded differently: Proliferation increased up to a WSS of 17.5 Pa but decreased under higher WSS. Proliferation was significantly different between positive and negative WSSG when WSS was above 17.5 Pa (for WSS of 17.5–20 Pa, $p = 0.05$; 20–22.5 Pa, $p = 0.01$; 22.5–25 Pa, $p = 0.01$; and 25–27.5 Pa, $p = 0.04$). Thus, positive and negative WSSG have different effects on growth in very high WSS environments.

TUNEL staining revealed that the percentage of apoptotic cells was higher under positive WSSG than under negative WSSG for almost all WSS values (Fig. 8b). ECs exposed to negative WSSG had similar apoptotic levels to cells exposed to a WSS of 3.5 Pa and no gradient, whereas ECs exposed to positive WSSG had apoptotic levels that were similar to or higher than cells under 28.4 Pa and no gradient (Fig. 8b). Within the regions where positive and negative gradient were constant and of similar magnitude, apoptosis was significantly higher under positive WSSG than under negative WSSG for WSS of 12.5– 15, 15–17.5, and 20–22.5 Pa ($p = 0.03$, $p = 0.02$, and $p = 0.04$, respectively). Apoptosis was also higher under positive WSSG for WSS of 17.5–20 Pa, but the difference was not statistically significant at 95% confidence levels ($p = 0.09$).

DISCUSSION

High WSS is associated with expansive vascular remodeling throughout the vascular tree and with aneurysmal remodeling within the cerebral vasculature. However, endothelial responses to high WSS have not been well characterized. In the new flow system described here, we studied ECs exposed to WSS up to 28.4 Pa, a level that occurs commonly near the apices of bifurcations,[1,22] but to our knowledge has never been studied *in vitro*. Furthermore, the converging/diverging design of our flow chamber allows systematic study of cells in well-defined spatial gradients of WSS for both accelerating and decelerating flows. By creating regions of uniform gradient that occur over the same distance and the same range of WSS values, we can compare cell responses to WSSG that have very similar magnitude, but differ only in the sign of the gradient. Through this approach, we demonstrate that ECs distinguish between positive and negative WSSG. The responses of ECs to high WSS and to WSSG have potentially important biological implications, as discussed below.

Effects of High WSS

Exposing ECs to moderate WSS, equivalent to those experienced by endothelia under normal baseline flow in straight arterial segments, promotes a quiescent state, suppressing

proliferation and apoptosis compared to static or very low flow conditions.[11,20] In contrast, higher-than-baseline WSS could be expected to stimulate EC proliferation. *In vivo*, Sho *et al*. have shown that raising WSS to ~8.5 Pa in rabbit carotid arteries leads to adaptive expansion of the vessels, accompanied by an increase in the number of proliferating ECs from 0.01% in controls to 9% in high flow arteries, presumably to provide more ECs to maintain endothelial coverage over the larger surface.[35,36] We previously reported that WSS of 3–10 Pa stimulates proliferation in cultured ECs,[27] demonstrating that higher-than-baseline WSS can induce EC proliferation directly. The present study shows that this stimulation is maintained even under more extreme flow conditions equivalent to those found *in vivo* near bifurcation apices.[1,22] Interestingly, mitotic ECs in the aortic tree of guinea pigs are found almost exclusively around bifurcations,[46] suggesting that these high WSS regions may be sources of new ECs *in vivo*.

We previously observed that apoptosis in cultured ECs decreases as WSS increases from 2 to 10 Pa.[27] However, in the present study we found that WSS of 28.4 Pa *increased* apoptosis relative to lower WSS (3.5 Pa) conditions, suggesting a bimodal response to high WSS. There may be a threshold at which WSS switches from being a trophic and protective signal to having detrimental effects on ECs, perhaps causing mechanical damage to cell–cell junctions or cell surface integrity. Although the percentage of apoptosing cells we observed was small, it should be noted that the true number of cells lost to apoptosis is likely much higher, because dying cells are rapidly removed by flow. Furthermore, some cells that are not apoptotic may be lost through mechanical detachment, particularly when cells are rearranging their adhesions during elongation, re-orientation, or cell division. Even a small loss of cells can have significant effects on endothelial function *in vivo*, resulting in compromised barrier function allowing plasma proteins and circulating cells to enter the vessel wall. This may elicit wound-like responses within the vessel wall, such as matrix degradation and re-synthesis.

It may seem contradictory that high WSS would stimulate both proliferation and apoptosis at the same time. However, when arteries undergo expansive remodeling in response to elevated flow *in vivo*, endothelial proliferation is also accompanied by increased apoptosis.[5,38] This behavior might facilitate vessel remodeling by stimulating cell turnover and rearrangement and also replacing weaker cells in the endothelium.

Contrasting Effects of Positive and Negative WSSG

The behavior of ECs in the converging and diverging regions of our chamber indicates that the effects of high WSS on alignment, proliferation, and apoptosis can be exacerbated or ameliorated by WSSG. It is particularly noteworthy that accelerating flow and decelerating flow over the same WSS values have different effects. Mechanically, accelerating flow creates a stretching force within the surface of the EC layer as the frictional drag increases from point to point in the direction of flow.[18,45] In contrast, decelerating flow will cause compression within the surface. These contrasting forces may augment or diminish, respectively, the stretch already exerted *across* the endothelial layer by high WSS as it pulls the endothelial surface downstream relative to EC-substratum adhesions. Such forces could affect EC behavior by disrupting cell–cell junctions and communication, activating

intracellular signaling via conformational changes in junctional or cytoskeletal proteins,[42] or by modulating stretch-activated ion channels.[4]

WSSG Combined with High WSS

It has been speculated that WSSG in conjunction with low WSS plays an important role in atherosclerosis. This is because atherosclerotic lesions preferentially localize to low flow regions that experience disturbed flow, which creates temporal and spatial WSSG. When ECs are exposed to a region of low WSS and large spatial WSSG using flow over a backward-facing step, they exhibit altered transendothelial permeability,[31] disruption of tight and gap junctions,[9,41] and increased migration, proliferation, cell loss,[10,40] and activation of transcription factors.[29] However, such studies did not compare the response of ECs to low shear stress alone, so the effects of WSS vs. WSSG were not isolated. LaMack *et al*.[18] analyzed the expression of five atherosclerosis-related genes in ECs exposed to WSS values ranging from 0.6 to 4.8 Pa and positive gradients up to 500 Pa/m. Multivariate analysis of gene expression as a function of WSS and WSSG revealed that WSSG had effects on the expression of c-jun, ICAM-1, and MCP-1 above and beyond the effects of WSS alone. eNOS expression was dependent only on WSS, and VCAM-1 was independent of both forces. Thus, ECs can sense WSSG and WSS independently, and these two forces can elicit differential responses even when WSS is quite low.

Our study shows that in *high* WSS conditions, positive WSSG appears to exacerbate EC dysfunction, whereas negative WSSG ameliorates it. Specifically, ECs under positive WSSG did not align as well, were more apoptotic, and had lower cell densities than ECs under negative WSSG at the same WSS. Inhibition of flow-induced alignment in regions of positive WSSG has also been observed when EC cultures are subjected to impinging flow.[33,39] The mechanism and significance of flow-induced alignment is unknown, but ECs do align parallel to flow in straight arteries *in vivo* and notably exhibit disrupted alignment near the apices of bifurcations,[32] where WSS is high and strong positive WSSG occurs.

Another indication that positive WSSG exacerbates EC dysfunction is the lower EC density under positive WSSG. Cell density was lower at all values of WSS under positive WSSG when compared to negative WSSG. Furthermore, the density of cells under positive WSSG was lower than that of cells under no gradient regardless of whether the no-gradient cells were subjected to 3.5 or 28.4 Pa of WSS. The lower density occurs despite higher levels of proliferation. This can be explained by higher levels of cell loss and turnover in the positive WSSG regions. In fact, we also found higher rates of apoptosis under positive WSSG. Because the normal behavior of ECs is to grow until becoming a confluent monolayer and then become quiescent, high turnover suggests endothelial dysfunction.

Evidence for endothelial dysfunction *in vivo* under high WSS/positive WSSG conditions has been observed in two animal systems: during initiation of aneurysms by increasing flow at the basilar bifurcation in rabbits,[25,28] and adjacent to the *de novo* apex of surgically created bifurcations in canine carotid arteries.[26,45] In both systems, destructive remodeling is localized to regions of elevated WSS and positive WSSG, while regions immediately downstream of the damage, which experience equally high WSS but a negative WSSG, appear normal. Localized EC dysfunction induced by high WSS/high WSSG could

contribute to destructive remodeling by disrupting endothelial barrier function or by diminishing endothelial signals that maintain vessel homeostasis. Reduced expression of endothelial nitric oxide synthase—a common molecular marker for EC dysfunction—has been reported in the high WSS/positive WSSG region of the surgically created bifurcations,[45] and we have observed EC apoptosis and loss of the EC junctional protein PECAM-1 in the corresponding region of the rabbit basilar bifurcations subjected to increased flow[16]. Such endothelial dysfunction may be the beginning of destructive remodeling leading to aneurysm formation. These potential endothelial responses to high WSS/positive WSSG warrant further investigation *in vivo*.

The present study demonstrates that ECs are sensitive to the magnitude of WSS, the spatial gradient in WSS, and the sign of the gradient. The interaction between these different hemodynamic forces produces different effects in high WSS environments than what has been previously reported in low WSS conditions. These unique responses, affecting EC alignment, proliferation, and apoptosis, have potentially important implications for vascular remodeling both in maintaining homeostasis (e.g., during accommodation of a chronic flow increase) and in maladaptive responses (e.g., initiation of cerebral aneurysm). The system described will permit analysis of the molecular mechanism by which these particular flow conditions elicit specific responses from ECs.

Acknowledgments

We thank Eleni Metaxa for contributions to chamber design and stimulating discussions, Robert Baier for critical advice on biocompatible materials, Scott Woodward for technical assistance in chamber design, Nicholas Liaw for stimulating discussions, and Jianping Xiang for assistance with CFD. We also acknowledge the assistance of Wade Sigurdson and the Confocal Microscope and Flow Cytometry Core Facility at the University of Buffalo. This work was supported by the NIH grant R01NS064592 (H.M.) and the American Society for Quality (J.D.).

REFERENCES

1. Alnaes MS, Isaksen J, Mardal KA, Romner B, Morgan MK, Ingebrigtsen T. Computation of hemodynamics in the circle of Willis. Stroke. 2007; 38:2500–2505. [PubMed: 17673714]
2. Bacabac RG, Smit TH, Cowin SC, Van Loon JJ, Nieuwstadt FT, Heethaar R, Klein-Nulend J. Dynamic shear stress in parallel-plate flow chambers. J. Biomech. 2005; 38:159–167. [PubMed: 15519352]
3. Baier RE. Surface behaviour of biomaterials: the theta surface for biocompatibility. J. Mater. Sci. Mater. Med. 2006; 17:1057–1062. [PubMed: 17122919]
4. Brakemeier S, Eichler I, Hopp H, Kohler R, Hoyer J. Up-regulation of endothelial stretch-activated cation channels by fluid shear stress. Cardiovasc. Res. 2002; 53:209–218. [PubMed: 11744030]
5. Buus CL, Pourageaud F, Fazzi GE, Janssen G, Mulvany MJ, De Mey JG. Smooth muscle cell changes during flow-related remodeling of rat mesenteric resistance arteries. Circ. Res. 2001; 89:180–186. [PubMed: 11463726]
6. Chaudhuri S, Nguyen H, Rangayyan RM, Walsh S, Frank CB. A Fourier domain directional filtering method for analysis of collagen alignment in ligaments. IEEE Trans. Biomed. Eng. 1987; 34:509–518. [PubMed: 3610201]
7. Chien S. Mechanotransduction and endothelial cell homeostasis: the wisdom of the cell. Am. J. Physiol. Heart Circ. Physiol. 2007; 292:H1209–H1224. [PubMed: 17098825]
8. Davies PF. Flow-mediated endothelial mechanotrans-duction. Physiol. Rev. 1995; 75:519–560. [PubMed: 7624393]

9. DePaola N, Davies PF, Pritchard WF Jr, Florez L, Harbeck N, Polacek DC. Spatial and temporal regulation of gap junction connexin43 in vascular endothelial cells exposed to controlled disturbed flows in vitro. Proc. Natl. Acad. Sci. USA. 1999; 96:3154–3159. [PubMed: 10077653]
10. DePaola N, Gimbrone MA Jr, Davies PF, Dewey CF Jr. Vascular endothelium responds to fluid shear stress gradients. Arterioscler. Thromb. 1992; 12:1254–1257. [PubMed: 1420084]
11. Dimmeler S, Haendeler J, Rippmann V, Nehls M, Zeiher AM. Shear stress inhibits apoptosis of human endothelial cells. FEBS Lett. 1996; 399:71–74. [PubMed: 8980122]
12. Gimbrone MA Jr, Topper JN, Nagel T, Anderson KR, Garcia-Cardena G. Endothelial dysfunction, hemodynamic forces, and atherogenesis. Ann. N. Y. Acad. Sci. 2000; 902:230–239. discussion 239–240. [PubMed: 10865843]
13. Jou LD, van Tyen R, Berger SA, Saloner D. Calculation of the magnetization distribution for fluid flow in curved vessels. Magn. Reson. Med. 1996; 35:577–584. [PubMed: 8992209]
14. Kolega J. Cytoplasmic dynamics of myosin IIA and IIB: spatial 'sorting' of isoforms in locomoting cells. J. Cell Sci. 1998; 111(Pt 15):2085–2095. [PubMed: 9664030]
15. Kolega J. Asymmetric distribution of myosin IIB in migrating endothelial cells is regulated by a rho-dependent kinase and contributes to tail retraction. Mol. Biol. Cell. 2003; 14:4745–4757. [PubMed: 12960430]
16. Kolega J, Gao L, Mandelbaum M, Mocco J, Siddiqui AH, Natarajan SK, Meng H. Cellular and molecular responses of the basilar terminus to hemodynamics during intracranial aneurysm initiation in a rabbit model. J. Vasc. Res. 2011 in press.
17. Krex D, Schackert HK, Schackert G. Genesis of cerebral aneurysms—an update. Acta Neurochir. (Wien). 2001; 143:429–448. discussion 448–429. [PubMed: 11482693]
18. LaMack JA, Friedman MH. Individual and combined effects of shear stress magnitude and spatial gradient on endothelial cell gene expression. Am. J. Physiol. Heart Circ. Physiol. 2007; 293:H2853–H2859. [PubMed: 17766484]
19. Lehoux S, Tronc F, Tedgui A. Mechanisms of blood flow-induced vascular enlargement. Biorheology. 2002; 39:319–324. [PubMed: 12122247]
20. Levesque MJ, Nerem RM, Sprague EA. Vascular endothelial cell proliferation in culture and the influence of flow. Biomaterials. 1990; 11:702–707. [PubMed: 2090307]
21. Li X, Kolega J. Effects of direct current electric fields on cell migration and actin filament distribution in bovine vascular endothelial cells. J. Vasc. Res. 2002; 39:391–404. [PubMed: 12297702]
22. Lindekleiv HM, Valen-Sendstad K, Morgan MK, Mardal KA, Faulder K, Magnus JH, Waterloo K, Romner B, Ingebrigtsen T. Sex differences in intra-cranial arterial bifurcations. Gend. Med. 2010; 7:149–155. [PubMed: 20435277]
23. Malek AM, Alper SL, Izumo S. Hemodynamic shear stress and its role in atherosclerosis. JAMA. 1999; 282:2035–2042. [PubMed: 10591386]
24. Martins GG, Kolega J. Endothelial cell protrusion and migration in three-dimensional collagen matrices. Cell Motil. Cytoskelet. 2006; 63:101–115.
25. Meng H, Metaxa E, Gao L, Liaw N, Natarajan SK, Swartz DD, Siddiqui AH, Kolega J, Mocco J. Progressive aneurysm development following hemodynamic insult. J. Neurosurg. 2011 in press.
26. Meng H, Wang Z, Hoi Y, Gao L, Metaxa E, Swartz DD, Kolega J. Complex hemodynamics at the apex of an arterial bifurcation induces vascular remodeling resembling cerebral aneurysm initiation. Stroke. 2007; 38:1924–1931. [PubMed: 17495215]
27. Metaxa E, Meng H, Kaluvala SR, Szymanski MP, Paluch RA, Kolega J. Nitric oxide-dependent stimulation of endothelial cell proliferation by sustained high flow. Am. J. Physiol. Heart Circ. Physiol. 2008; 295:H736–H742. [PubMed: 18552158]
28. Metaxa E, Tremmel M, Natarajan SK, Xiang J, Paluch RA, Mandelbaum M, Siddiqui AH, Kolega J, Mocco J, Meng H. Characterization of critical hemodynamics contributing to aneurysmal remodeling at the basilar terminus in a rabbit model. Stroke. 2010; 41:1774–1782. [PubMed: 20595660]
29. Nagel T, Resnick N, Dewey CF Jr, Gimbrone MA Jr. Vascular endothelial cells respond to spatial gradients in fluid shear stress by enhanced activation of transcription factors. Arterioscler. Thromb. Vasc. Biol. 1999; 19:1825–1834.

30. Ng CP, Hinz B, Swartz MA. Interstitial fluid flow induces myofibroblast differentiation and collagen alignment in vitro. J. Cell Sci. 2005; 118:4731–4739. [PubMed: 16188933]
31. Phelps JE, DePaola N. Spatial variations in endothelial barrier function in disturbed flows in vitro. Am. J. Physiol. Heart Circ. Physiol. 2000; 278:H469–H476. [PubMed: 10666077]
32. Reidy MA, Langille BL. The effect of local blood flow patterns on endothelial cell morphology. Exp. Mol. Pathol. 1980; 32:276–289. [PubMed: 7379981]
33. Sakamoto N, Saito N, Han X, Ohashi T, Sato M. Effect of spatial gradient in fluid shear stress on morphological changes in endothelial cells in response to flow. Biochem. Biophys. Res. Commun. 2010; 395:264–269. [PubMed: 20371223]
34. Schirmer CM, Malek AM. Wall shear stress gradient analysis within an idealized stenosis using non-Newtonian flow. Neurosurgery. 2007; 61:853–863. discussion 863–854. [PubMed: 17986948]
35. Sho E, Komatsu M, Sho M, Nanjo H, Singh TM, Xu C, Masuda H, Zarins CK. High flow drives vascular endothelial cell proliferation during flow-induced arterial remodeling associated with the expression of vascular endothelial growth factor. Exp. Mol. Pathol. 2003; 75:1–11. [PubMed: 12834620]
36. Sho E, Sho M, Singh TM, Nanjo H, Komatsu M, Xu C, Masuda H, Zarins CK. Arterial enlargement in response to high flow requires early expression of matrix metalloproteinases to degrade extracellular matrix. Exp. Mol. Pathol. 2002; 73:142–153. [PubMed: 12231217]
37. Stone PH, Coskun AU, Yeghiazarians Y, Kinlay S, Popma JJ, Kuntz RE, Feldman CL. Prediction of sites of coronary atherosclerosis progression: in vivo profiling of endothelial shear stress, lumen, and outer vessel wall characteristics to predict vascular behavior. Curr. Opin. Cardiol. 2003; 18:458–470. [PubMed: 14597887]
38. Sullivan CJ, Hoying JB. Flow-dependent remodeling in the carotid artery of fibroblast growth factor-2 knockout mice. Arterioscler. Thromb. Vasc. Biol. 2002; 22:1100–1105. [PubMed: 12117723]
39. Szymanski MP, Metaxa E, Meng H, Kolega J. Endothelial cell layer subjected to impinging flow mimicking the apex of an arterial bifurcation. Ann. Biomed. Eng. 2008; 36:1681–1689. [PubMed: 18654851]
40. Tardy Y, Resnick N, Nagel T, Gimbrone MA Jr, Dewey CF Jr. Shear stress gradients remodel endothelial monolayers in vitro via a cell proliferation-migration-loss cycle. Arterioscler. Thromb. Vasc. Biol. 1997; 17:3102–3106. [PubMed: 9409299]
41. Thi MM, Tarbell JM, Weinbaum S, Spray DC. The role of the glycocalyx in reorganization of the actin cytoskeleton under fluid shear stress: a “bumper-car” model. Proc. Natl. Acad. Sci. USA. 2004; 101:16483–16488. [PubMed: 15545600]
42. Tzima E, Irani-Tehrani M, Kiosses WB, Dejana E, Schultz DA, Engelhardt B, Cao G, DeLisser H, Schwartz MA. A mechanosensory complex that mediates the endothelial cell response to fluid shear stress. Nature. 2005; 437:426–431. [PubMed: 16163360]
43. van Everdingen KJ, Klijn CJ, Kappelle LJ, Mali WP, van der Grond J. MRA flow quantification in patients with a symptomatic internal carotid artery occlusion. The Dutch EC-IC Bypass Study Group. Stroke. 1997; 28:1595–1600. [PubMed: 9259755]
44. Viggers RF, Wechezak AR, Sauvage LR. An apparatus to study the response of cultured endothelium to shear stress. J. Biomech. Eng. 1986; 108:332–337. [PubMed: 3795878]
45. Wang Z, Kolega J, Hoi Y, Gao L, Swartz DD, Levy EI, Mocco J, Meng H. Molecular alterations associated with aneurysmal remodeling are localized in the high hemodynamic stress region of a created carotid bifurcation. Neurosurgery. 2009; 65:169–177. discussion 177–168. [PubMed: 19574839]
46. Wright HP. Endothelial mitosis around aortic branches in normal guinea pigs. Nature. 1968; 220:78–79. [PubMed: 5677450]
47. Zarins CK, Giddens DP, Bharadvaj BK, Sottiurai VS, Mabon RF, Glagov S. Carotid bifurcation atherosclerosis. Quantitative correlation of plaque localization with flow velocity profiles and wall shear stress. Circ. Res. 1983; 53:502–514. [PubMed: 6627609]

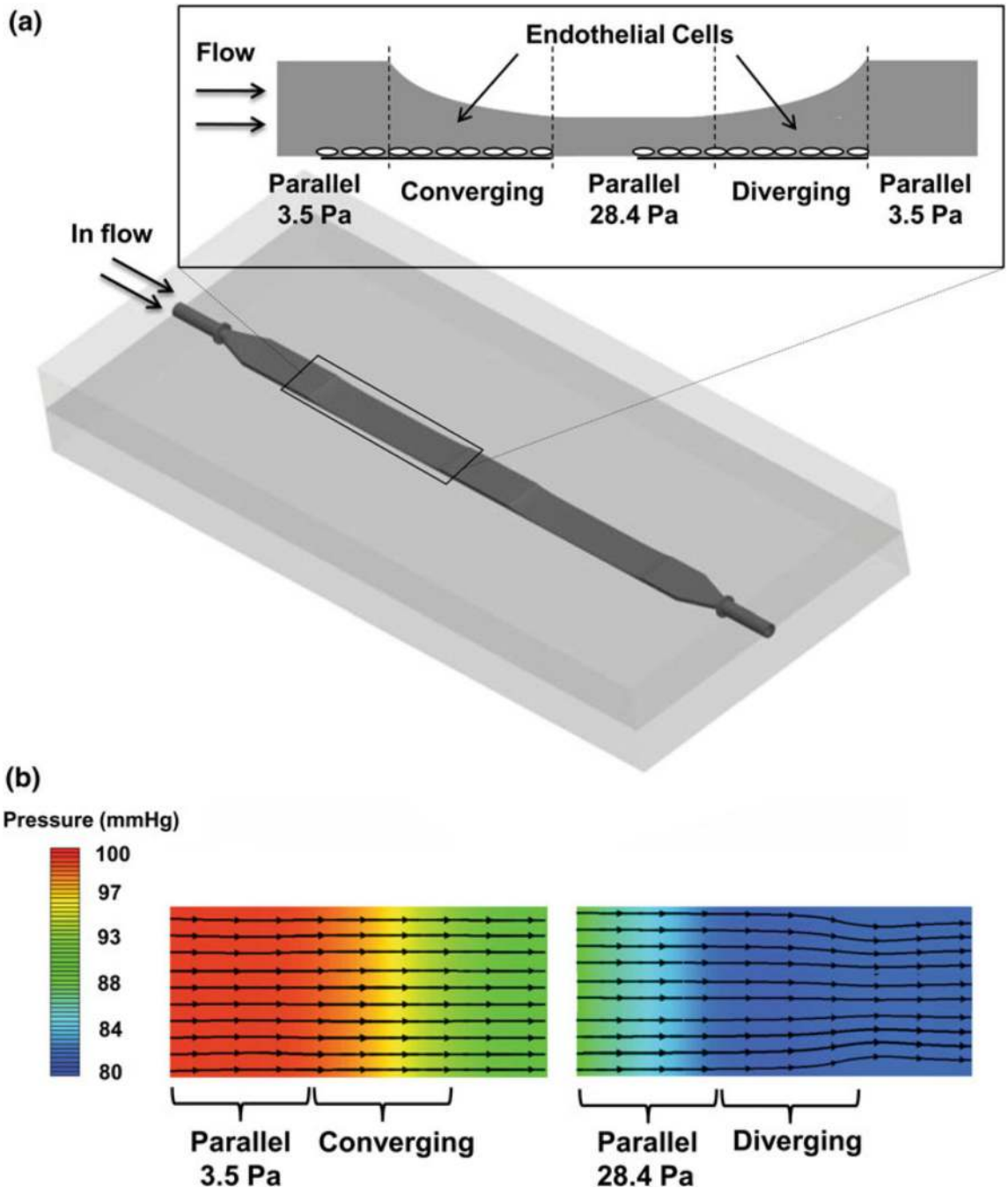

FIGURE 1.

(a) Schematic of the flow chamber. Flow enters a parallel section (uniform WSS, zero WSSG regime), converges (positive WSSG regime) to a second parallel section (high WSS, zero WSSG regime), and then diverges (negative WSSG regime) back to its original height. (b) Streamlines and pressure map of the bottom surface of the chamber. Cells are placed in the four bracketed regions. Slight convergence of streamlines is observed as flow exits the diverging region downstream of the last test section, but streamlines are largely parallel over almost all of the channel where cultured cells are located.

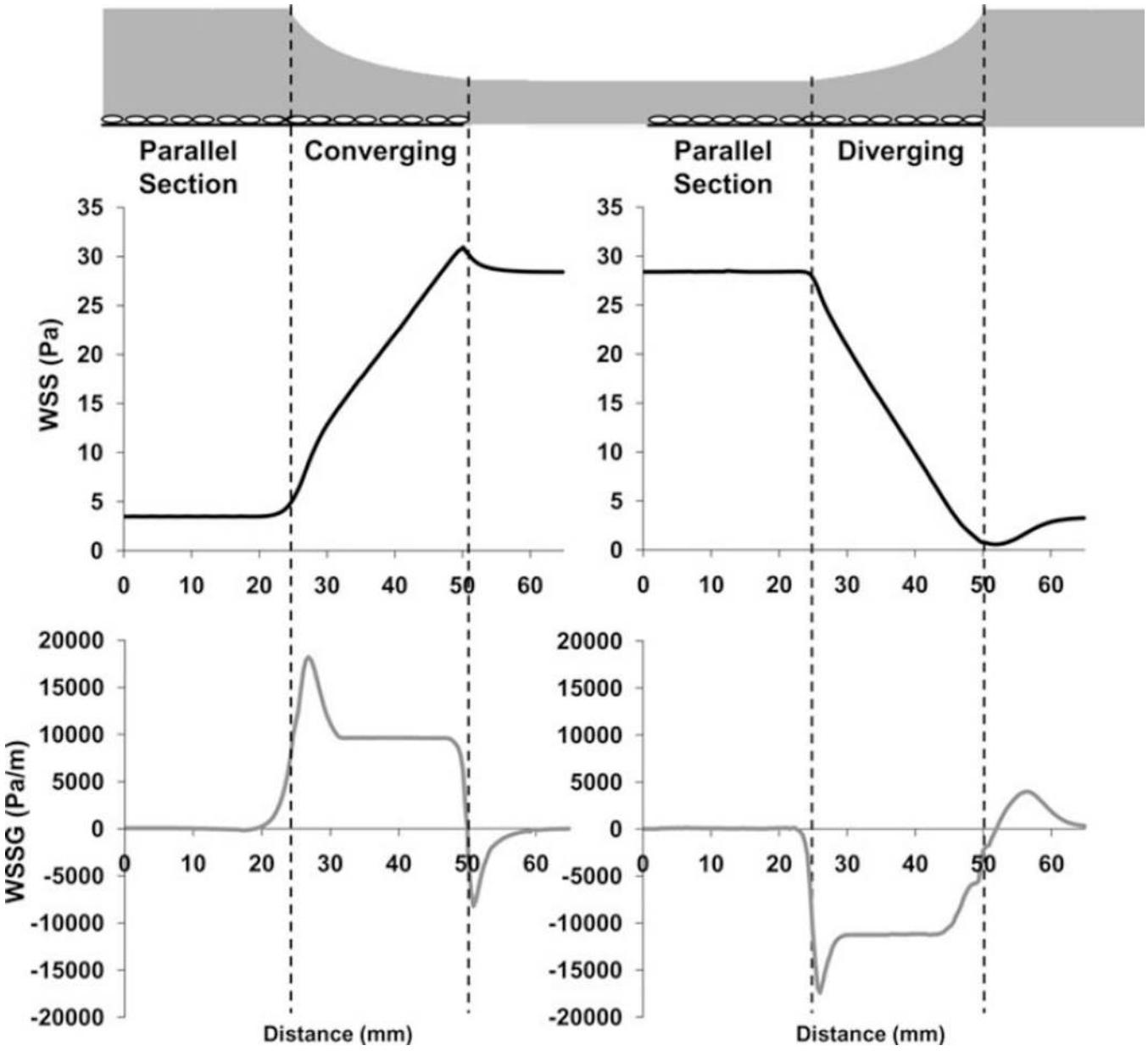

FIGURE 2.

WSS and WSSG distribution in the chamber. Flow enters a parallel section (WSS = 3.5 Pa, WSSG = 0) and then accelerates in a converging section (WSS increases, WSSG > 0). For WSS of 12.4–28.3 Pa, a constant positive gradient, WSSG = 980 Pa/m, is created in the converging section. Flow enters a second parallel section (WSS = 28.4 Pa, WSSG = 0) and then decelerates in a diverging section (WSS decreases, WSSG < 0). For WSS of 22.5–6.6 Pa, a constant negative gradient, WSSG = −1120 Pa/m, is created in the diverging section.

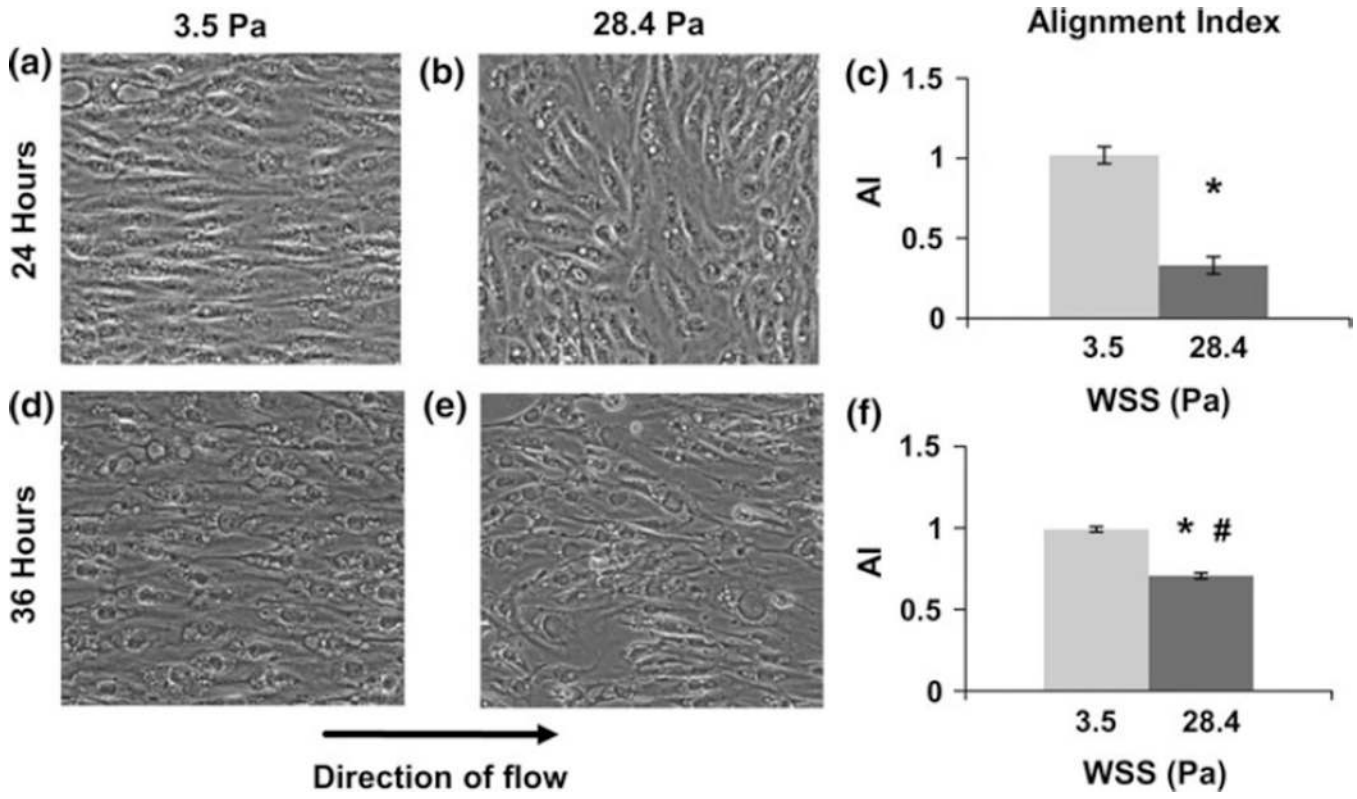

FIGURE 3.

EC morphology and orientation under high WSS. At 24 h of flow exposure (a–c), phase contrast images of ECs show (a) cell alignment in the flow direction under shear stress of 3.5 Pa and (b) cells do not align with flow under 28.4 Pa. (c) Cell alignment indices calculated from four independent experiments have significantly different values between these two WSS conditions. At 36 h of flow exposure, (d–f), phase contrast image shows that (d) ECs under 3.5 Pa remain aligned in the flow direction, while (e) those under the high shear stress of 28.4 Pa are not as aligned, albeit more aligned to the flow direction compared to 24 h. This is reflected in the cell alignment indices in (f), calculated from three independent experiments. Bars represent mean ± SE. *indicates statistically significant difference between 3.5 and 28.4 Pa (mixed model ANOVA, $p<0.007$). $^{\#}$indicates statistically significant difference between 24 and 36 h under the same shear stress (mixed model ANOVA, $p = 0.04$).

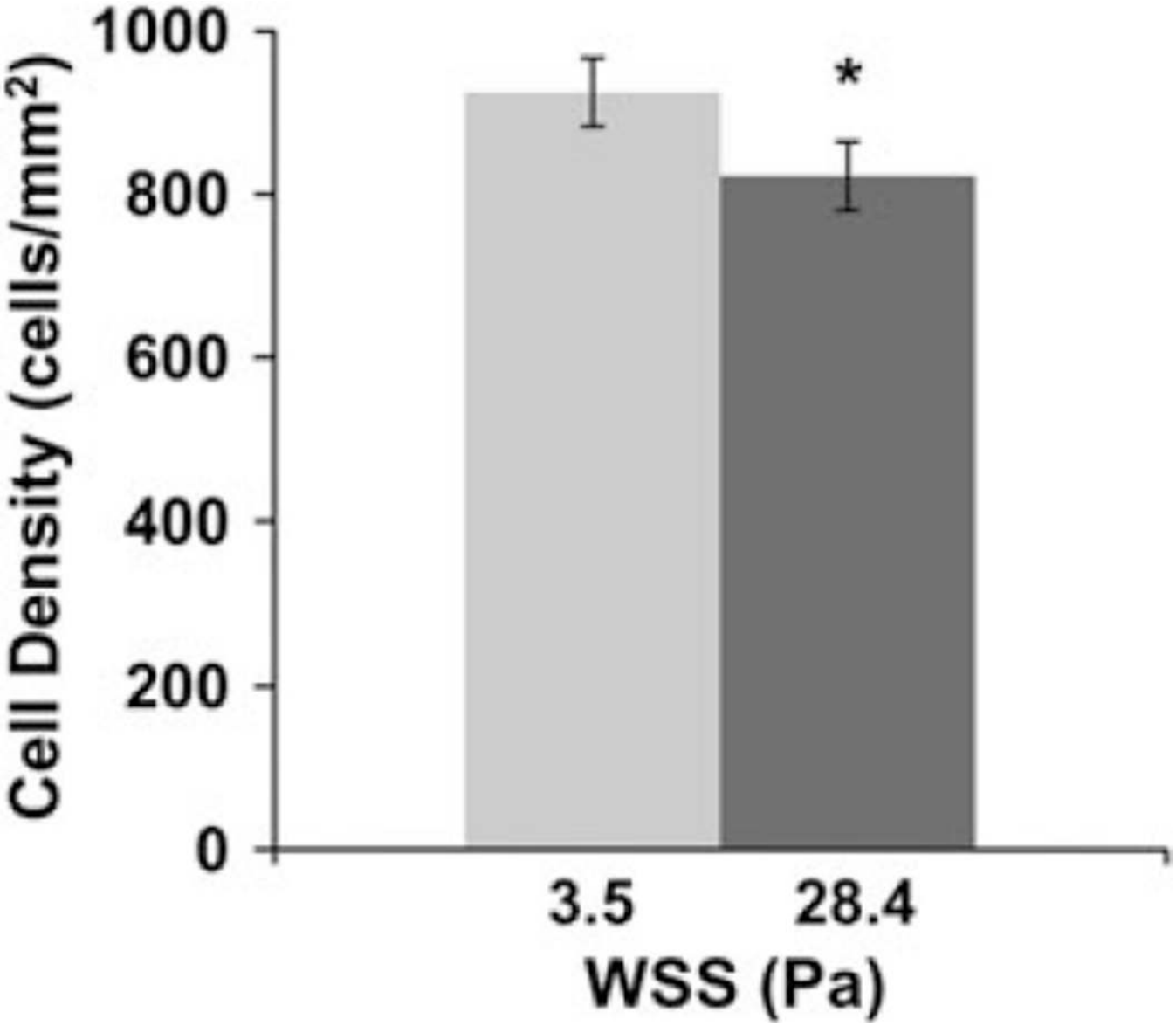

FIGURE 4.

Cell density measurements at 24 h. Cell density was significantly lower under 28.4 Pa. Bar graphs represent the average of six experiments ± SE. *indicates statistically significant difference from 3.5 Pa (mixed model ANOVA, $p = 0.0001$).

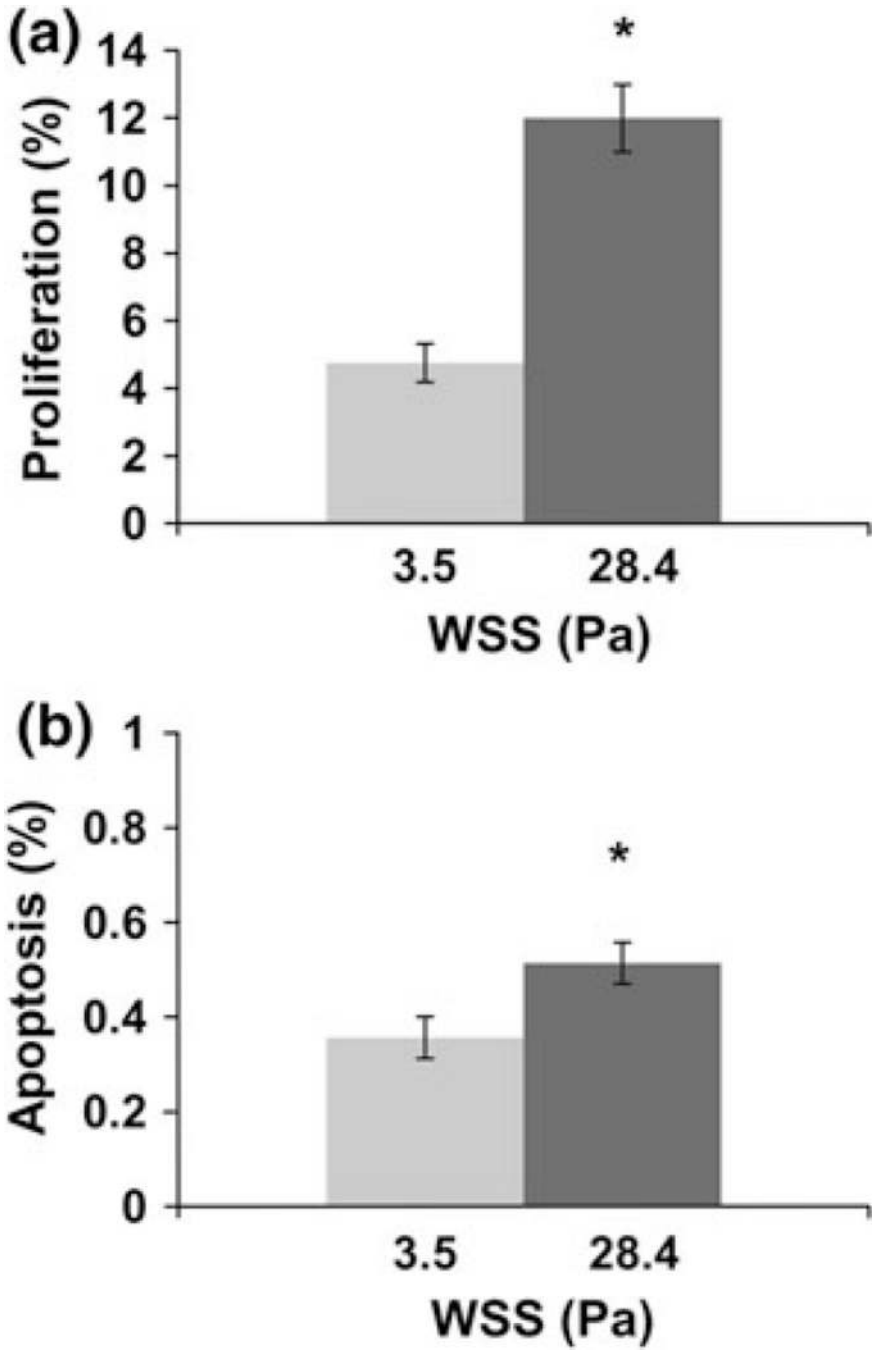

FIGURE 5.

Percentage of ECs undergoing proliferation and apoptosis after 24 h. (a) Percentage of proliferating cells significantly increased when WSS was 28.4 Pa. Bar graphs represent the mean of three experiments ± SE. (b) Percentage of apoptotic cells significantly increased under 28.4 Pa. Bar graphs represent the average of four experiments ± SE. *indicates statistically significant difference from 3.5 Pa (mixed model ANOVA, $p < 0.02$).

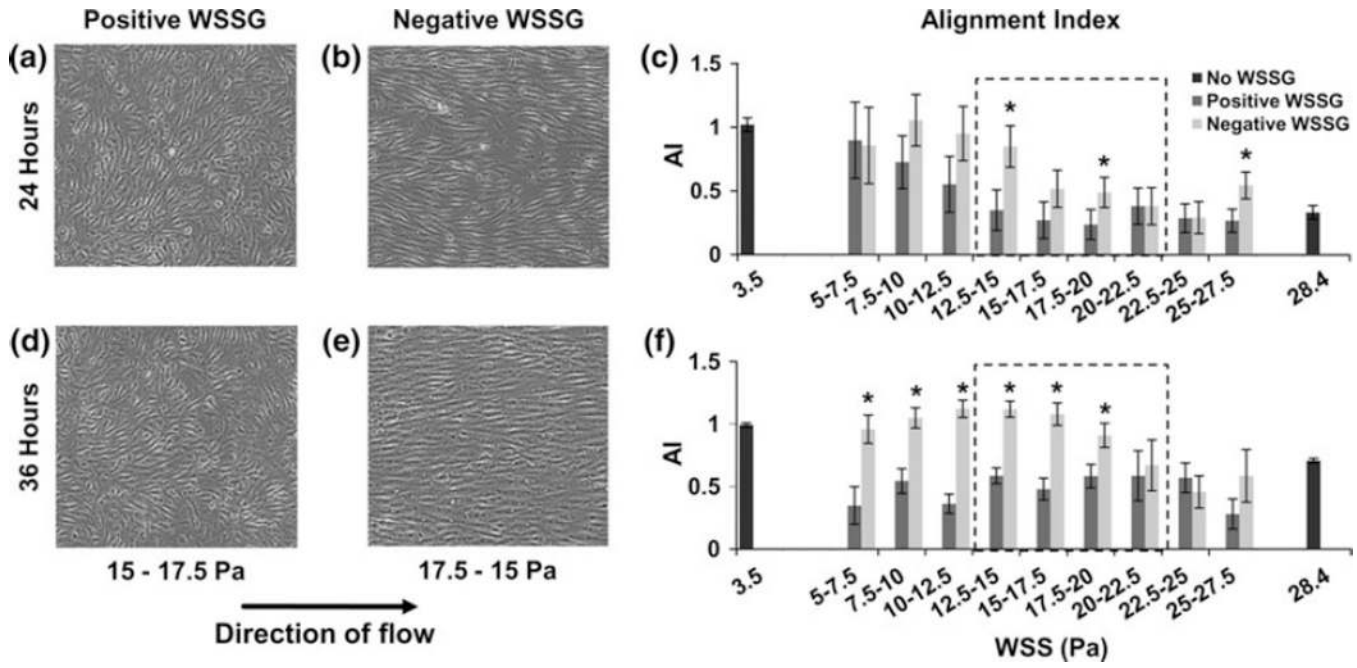

FIGURE 6.

EC alignment under accelerating (positive WSSG) and decelerating flow (negative WSSG) at 24 h (a–c) and 36 h (d–f). (a, b, d, e) Phase contrast images of ECs in a band with WSS ranging from 15 to 17.5 Pa either in the converging section with positive WSSG (a, d) or in the diverging section with negative WSSG (b, e). (c, f) Alignment indices for ECs located in the parallel sections and exposed to 3.5 and 28.4 Pa with no gradient (black bars) and for all ECs located in the converging section (positive WSSG, dark bars) and the diverging section (negative WSSG, light bars). Bar graphs represent the average of four experiments ± SE at 24 h (c) and the average of three experiments ± SE at 36 h (f). The dashed box indicates the zone where positive and negative WSSG are constant and similar magnitudes, *indicates statistically significant difference between positive WSSG and negative WSSG result (mixed model ANOVA, $p < 0.05$).

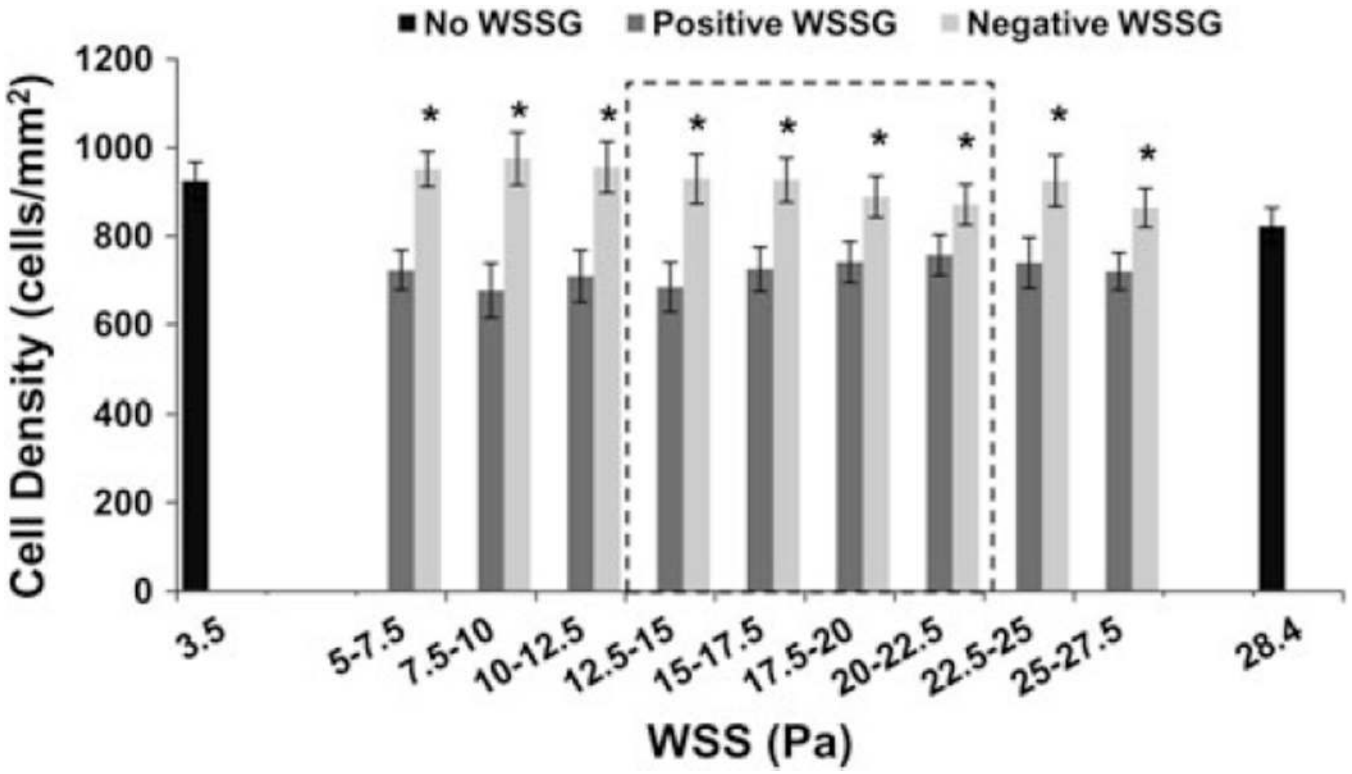

FIGURE 7.

Cell density measurements for ECs exposed to 3.5 and 28.4 Pa with no gradient (black bars) and to accelerating (positive WSSG, dark bars) and decelerating flow (negative WSSG, light bars) at 24 h. Bar graphs represent the average of six experiments ± SE. Dashed box represents the zone of constant positive and negative WSSG, *indicates statistically significant difference between positive WSSG and negative WSSG result (mixed model ANOVA, $p \leq 0.0003$).

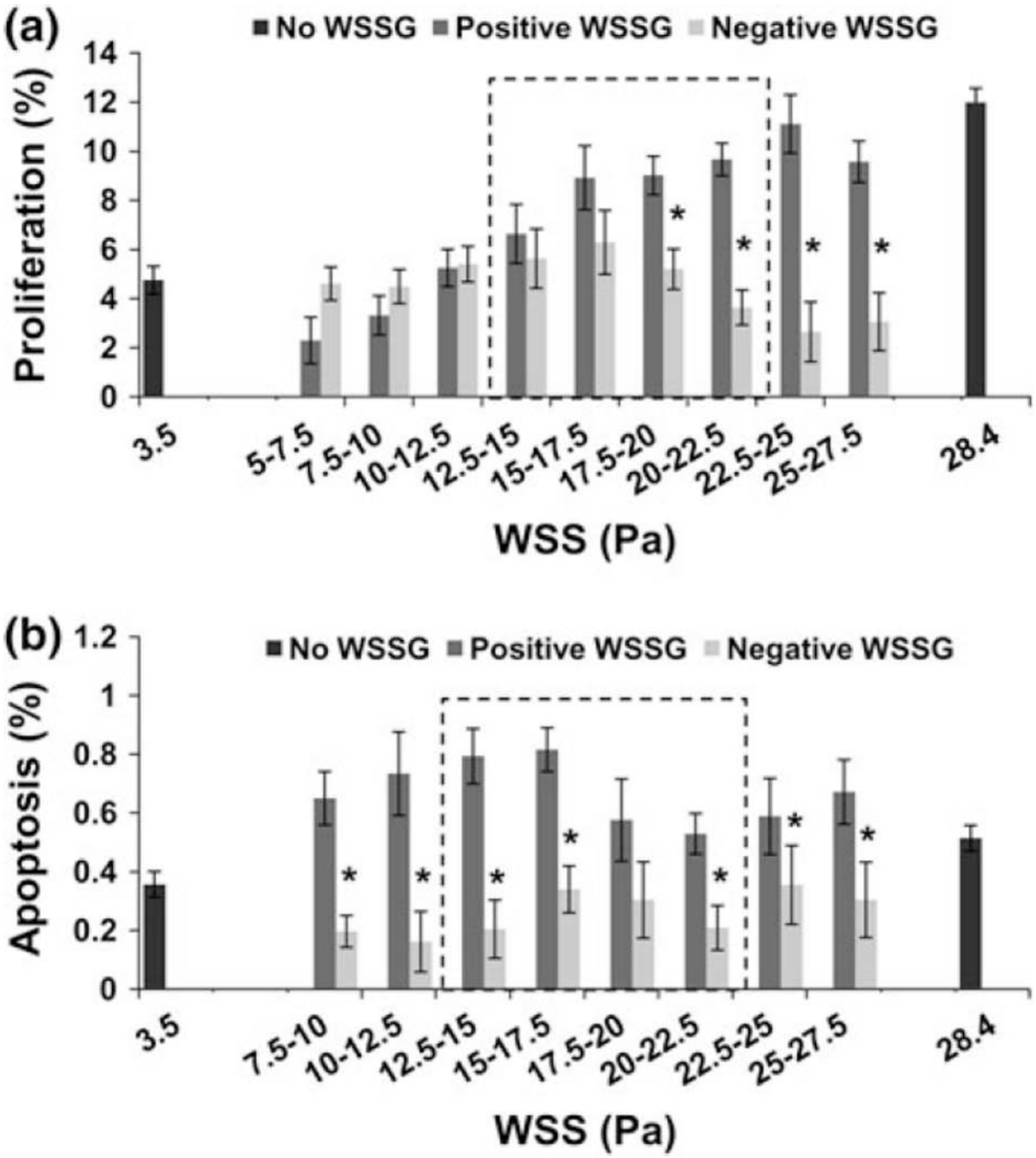

FIGURE 8.

Proliferation and apoptosis of EC under 3.5 and 28.4 Pa with no gradient (black bars) and accelerating (positive WSSG, dark bars) and decelerating flow (negative WSSG, light bars). (a) Proliferation after 24 h of flow. Bars represent the average of three experiments ± SE. (b) Apoptosis after 24 h of flow. Bars represent the average of four experiments ± SE. Dashed box indicates the zone where positive and negative WSSG are constant and similar

magnitude, *indicates statistically significant differences between positive and negative WSSG result (mixed model ANOVA, $p < 0.05$).